Available online at www.sciencedirect.com
ScienceDirect
Journal of the European Ceramic Society 31 (2011) 1631–1639
www.elsevier.com/locate/jeurceramsoc

UV laser microprocessing and post chemical etching on ultrathin Al_2O_3 ceramic substrate

Fei Zhang, Jun Duan *, Xiaoyan Zeng, Yu Cao

Division of Laser Science and Technology, Wuhan National Laboratory for Optoelectronics, School of Optoelectronics Science and Engineering, Huazhong University of Science and Technology, Wuhan, Hubei 430074, PR China

Received 27 July 2010; received in revised form 14 March 2011; accepted 20 March 2011
Available online 13 April 2011

Abstract

In this study, an Nd:YVO_4 UV laser was used for microprocessing ultrathin (125 μm) ceramic plates for use as a multi-layer microchip substrate. The effects of the UV laser microprocessing parameters, including laser power density, frequency, laser scanning speed, and pass delay on microprocessing accuracy and quality (kerf width and arithmetic average roughness R_a on the kerf sidewall) were investigated by means of a 4×4 orthogonal design. The key processing parameters were determined and optimized for small kerf width and minimal R_a of the kerf sidewall while retaining high production efficiency. Subsequent chemical etching of the laser processed areas was performed to reduce the kerf surface and kerf sidewall roughness by removing debris and the thin recast layer for the required size precision and post gilding treatment. The results showed that a clean surface and crack-free kerf sidewall with roughness R_a of 0.16 μm could be achieved by laser microprocessing and chemical etching.

Keywords: Laser microprocessing; Electron microscopy; Corrosion; Al_2O_3; Structural applications

1. Introduction

Ultrathin micro-ceramic parts are widely used in electronics, medicine, and micro-electro-mechanical systems (MEMS) as isolators, rigid supports, and as biocompatible components. The goals of microprocessing technology for ultrathin ceramic substrates are to simultaneously reduce production costs, while maintaining quality and production efficiency. Compared with traditional microprocessing methods, such as diamond grinding and ultrasonic microprocessing, laser microprocessing has a major advantage in the manufacture of complicated and ultrathin micro-ceramic parts due to its non-contact and high efficiency nature.[1,2] However, this technique also presents a number of problems, including micro-cracking in recast, micro-structural changes, heat affected zone (HAZ), and spatter of molten material onto the surface surrounding the processed areas. Some researchers focused on improving cutting quality of thick ceramics by using suitable laser parameters and shield gases.[3–6] In 2001, Modest[7] used a dual-beam arrangement to reduce thermal stresses by eliminating the sharpest temperature gradients. However, the secondary beam was able to substantially reduce the tensile stresses occurring ahead of the moving laser, but was unable to reduce the stresses to the sides of the scanning laser. Quintero et al.[8–10] reported that the microcracks on cut wall of mullite–alumina cutting were caused by the shrinkage of the molten ceramic during its cooling and only existed inside recast layer. The extension and the intensity of the HAZ were influenced by the laser parameters and the assist gas pressure only determined the beginning of the HAZ from the upper face of the workpiece. Over the past few years, new methods have been developed to reduce or eliminate the HAZ, debris, and micro-cracks that occur during the laser microprocessing of ceramic materials. Ji et al.[11] presented a close-piercing lapping (CPL) method of cutting thick Al_2O_3 ceramics up to 10 mm thick using a slab CO_2 laser and high-pressure assist gas. A crack-free cut surface with a roughness R_a of 31.74 μm could be attained by optimizing the processing parameters. However, there was still a recast layer on the cut edge, and the high-pressure assist gas was not suitable for ultrathin ceramic microprocessing. Kurita et al.[12] compared the nano-second and femto-second laser-processed surfaces of three kinds of ceramics, SiC, Si_3N_4 and Al_2O_3, and found that the quantity of debris created by

* Corresponding author. Fax: +86 27 87541423.
E-mail address: duans@mail.hust.edu.cn (J. Duan).

0955-2219/$ – see front matter © 2011 Elsevier Ltd. All rights reserved.
doi:10.1016/j.jeurceramsoc.2011.03.034

Table 1
Main parameters of the laser.

Laser parameters	Parameter range
Wavelength (nm)	355
Max. power (W)	7.5 (in the table)
Repetition frequency (kHz)	10–100
Power density (10^6 W/cm^2)	0–10.8
Pulse width (ns)	12–60
Quality factor (M^2)	<1.1

nano-second laser processing was much greater, underscoring the advantage of ultrashort (fs) laser-material interaction times. Perrie et al.[13] pointed out that melting could be minimised using ultrafast optical pulses, improving the edge quality. The debris produced consists mainly of single crystal nanoparticles of alumina with an average diameter of 300 nm. However, ultrafast laser systems are very expensive and the material removal rate is generally low, typically a few nanometers per pulse, because a high material removal rate also generates these problems mentioned above. Besides, there is still recast layer on the cut edge surface of the kerf bottom as the melting material cannot be removed inside deeper section. Some studies[14–16] attempted underwater laser processing or chemical assisted laser machining in order to alleviate the defects around the laser cut groove and reduce spatter deposition. Although the cooling effect of liquid can reduce the size of HAZ, recast layer and HAZ still exist, and the energy loss and the influence of bubbles, plasma, and shock waves on the processing are still disadvantages.

Most previous studies examined the creation of the recast layer during laser irradiation, or examined ways to reduce the size of the HAZ, while few attempted to remove the thin recast layer on the kerf sidewall and eliminate micro-cracks. In this work, a DPSS UV laser treatment was used to determine the key and optimal parameters that resulted in small kerf width and minimal R_a of the kerf sidewall with the highest efficiency. Subsequently, chemical etching was used to clean the debris on the kerf surface and remove the thin recast layer, thus reducing R_a to under 0.2 μm in order to satisfy the requirement for follow-up gilding on the kerf sidewall surface.

2. Experimental equipment, materials and methods

2.1. Experimental equipment and setup

The equipment used for this study includes a 355 nm DPSS Q-switched UV laser with average laser power of 7.5 W at a pulse repetition frequency of 25 kHz for the ultrathin ceramic surface (Fig. 1). A 2D galvanometer scanner controls laser beam to carry out the microprocessing. The main parameters of the UV laser used in the experiments are listed in Table 1. The laser has high stability, with both average power and pulse to pulse energy fluctuations of less than 2%. An ultrathin ceramic plate is fixed on a vacuum table by a clamper (Fig. 2). The focal plane is fixed on the surface of the samples and the laser beam spot size at focus is approximately

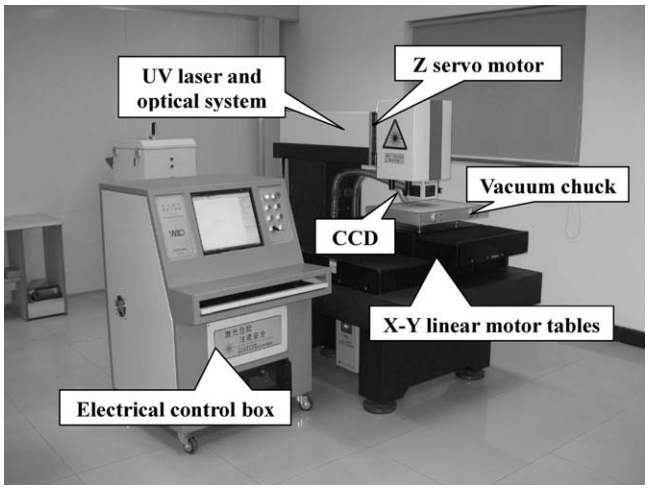

Fig. 1. UV laser microprocessing machine.

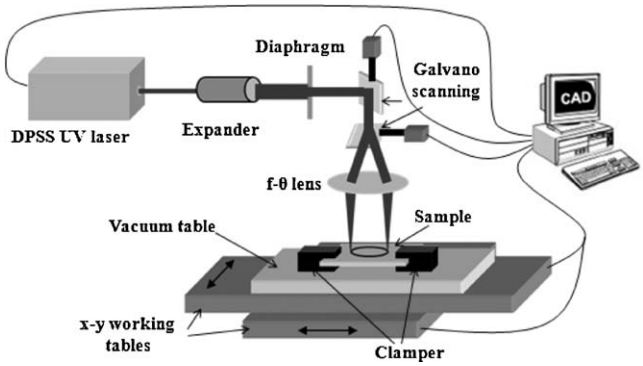

Fig. 2. Schematic diagram of experimental setup for UV laser microprocessing of ultrathin ceramics.

10 μm in diameter (and was used to calculate the laser power density).

2.2. Experimental material and microprocessing graphics

The physical properties of the 125 μm thick Al_2O_3 ceramics used in the experiments are listed in Table 2. The microprocessing graphics required on the ultrathin ceramic substrates were quite delicate and complex (Fig. 3), with many narrow slots and micro holes. The minimum slot width and hole diameter were 30 μm and 240 μm respectively. We surmised that laser microprocessing was the only method that could achieve the desired specifications due to the hardness and brittle nature of Al_2O_3 ceramics.

Table 2
Physical properties of the Al_2O_3 ceramic substrate.

Physical properties	Values
Thickness (μm)	125
Density (g/cm^3)	3.9
Hardness (HRA)	91
Modulus of elasticity (Gpa)	350
Fracture toughness (Mpa m$^{1/2}$)	4.5
Thermal expansion coefficient (10^{-6}/°C)	8.3

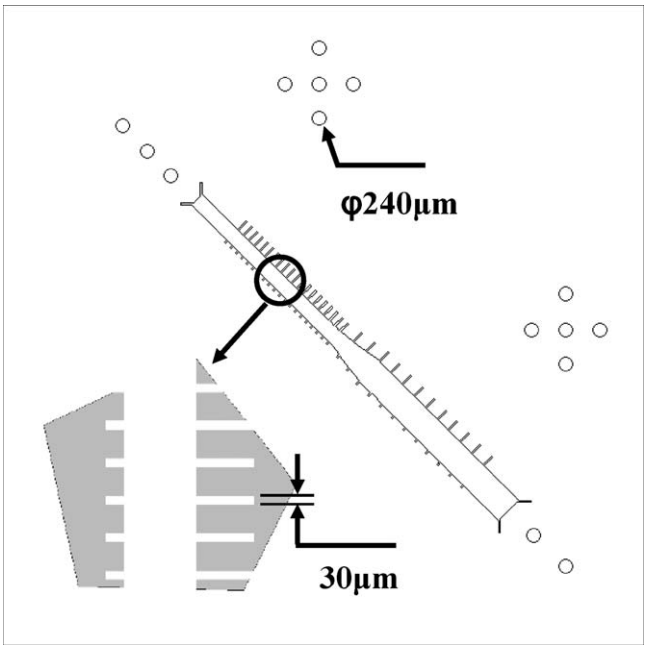

Fig. 3. The microprocessing graphics on the ultrathin ceramic.

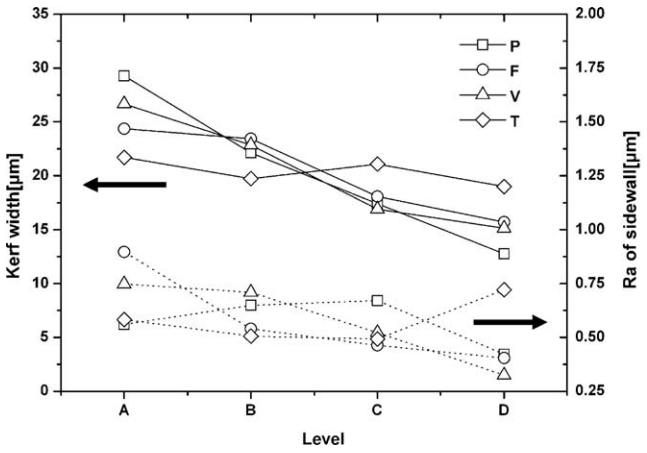

Fig. 4. The effect of different factors and levels on kerf width and R_a on the kerf sidewall.

2.3. Experimental method

A 4 × 4 orthogonal design was used to determine and optimize the key parameters for laser microprocessing of Al_2O_3 ceramics (Table 3). The effects of four factors on kerf width and sidewall roughness were evaluated: laser power density (P), frequency (F), laser scanning speed (V), and pass delay (T) (cooling time between each laser scan). Each factor was tested at four levels and the effects on both kerf width and roughness R_a of the kerf sidewall were determined. A laser multi-scan method was used to cut through the ceramic as this could greatly improve the processing quality and was suitable for processing with the high precision required. To maintain efficiency, the quotient of the laser scanning speed and the number of scans was held constant.

Table 3
Orthogonal design.

Levels	P (10^6 W/cm^2)	F (kHz)	V (mm/s)	T (ms)
A	5.09	25	5	0
B	4.45	40	30	200
C	3.81	60	200	400
D	3.17	70	1000	600

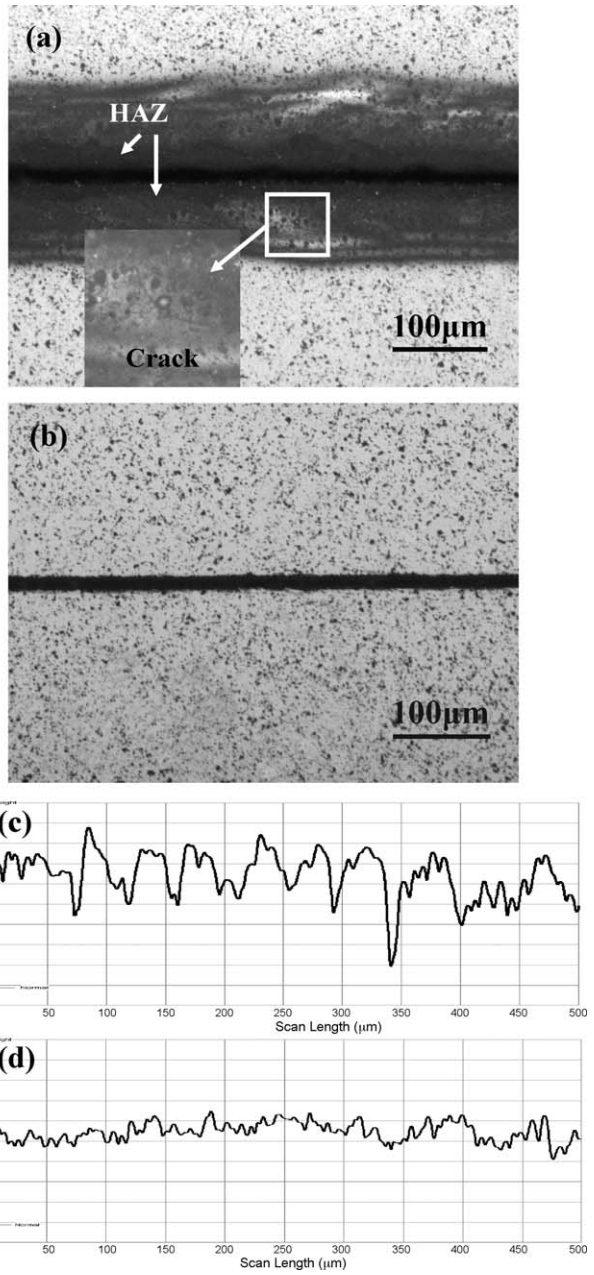

Fig. 5. Micrographs of kerf top and roughness profiles of sidewall: (a and c) 5.09 × 10^6 W/cm^2, 25 kHz, 5 mm/s; (b and d) 5.09 × 10^6 W/cm^2, 70 kHz, 1000 mm/s.

After UV laser processing, the samples were mounted in silicone so that the groove cross sections could be examined after cut, grinded and polished. Some of the samples were put in an ultrasonic cleaning machine (KQ2200DB, ultrasonic frequency 40 kHz, ultrasonic power 100 W) to study the effect of ultrasonic vibration. Some of the samples were soaked in 98% concentrated sulfuric acid, and heated in an oven at 100 °C for several hours

Table 4
The orthogonal experimental results.

No.	*P*	*F*	*V*	*T*	Kerf width (μm)	R_a (μm)
1	A	A	A	A	43.2	1.07
2	A	B	B	B	34.9	0.59
3	A	C	C	C	23.6	0.35
4	A	D	D	D	15.4	0.24
5	B	A	B	D	26.6	1.28
6	B	B	A	C	29.6	0.66
7	B	C	D	B	16.3	0.22
8	B	D	C	A	16.0	0.44
9	C	A	C	B	14.7	0.82
10	C	B	D	A	16.0	0.42
11	C	C	A	D	20.7	0.88
12	C	D	B	C	18.3	0.56
13	D	A	D	C	12.9	0.41
14	D	B	C	D	13.3	0.49
15	D	C	B	A	11.7	0.40
16	D	D	A	B	13.1	0.39

	Kerf width (μm)					R_a (μm)			
	P	*F*	*V*	*T*		*P*	*F*	*V*	*T*
W_A	29.28	24.35	26.65	21.73	R_A	0.56	0.90	0.75	0.58
W_B	22.13	23.45	22.88	19.75	R_B	0.65	0.54	0.71	0.51
W_C	17.43	18.08	16.90	21.10	R_C	0.67	0.46	0.53	0.50
W_D	12.75	15.70	15.15	19.00	R_D	0.42	0.41	0.32	0.72
R_W	16.53	8.65	11.50	2.73	R_R	0.25	0.49	0.43	0.22

after laser cutting to study the effects on the debris and rest layer. The characteristics of both kerf top surface and sidewall were investigated and analyzed using optical microscopy (Nikon Epiphot 300) and scanning electron microscopy (SEM, Quanta 200). The surface roughness of the kerf sidewall was examined by mechanical surface profiling (KLA TENCOR P16+).

3. Experimental results

3.1. UV laser microprocessing results

The orthogonal experimental results are given in Table 4. The values W_A to W_D present the average kerf widths of the four levels for each factor, and R_A to R_D indicate the average R_a values of the four levels. Values R_W and R_R are the ranges of W_A to W_D and R_A to R_D respectively, and reveal the maximum differences of the average values at different levels. The bigger the value of R_W or R_R, the more important the relevant factor is. The effects of different factors and levels on kerf width and sidewall roughness are shown in Fig. 4. The effects of *F* ($R_R = 0.49$) and *V* ($R_R = 0.43$) on the roughness were much greater than those of *P* ($R_R = 0.25$) or *T* ($R_R = 0.22$). It is noteworthy that as the laser frequency increased, the roughness on the kerf sidewall was reduced from 0.9 μm to 0.41 μm, while as the speed increased, the roughness R_a decreased from 0.75 μm to 0.32 μm. The influence of pass delay on sidewall roughness was not obvi-

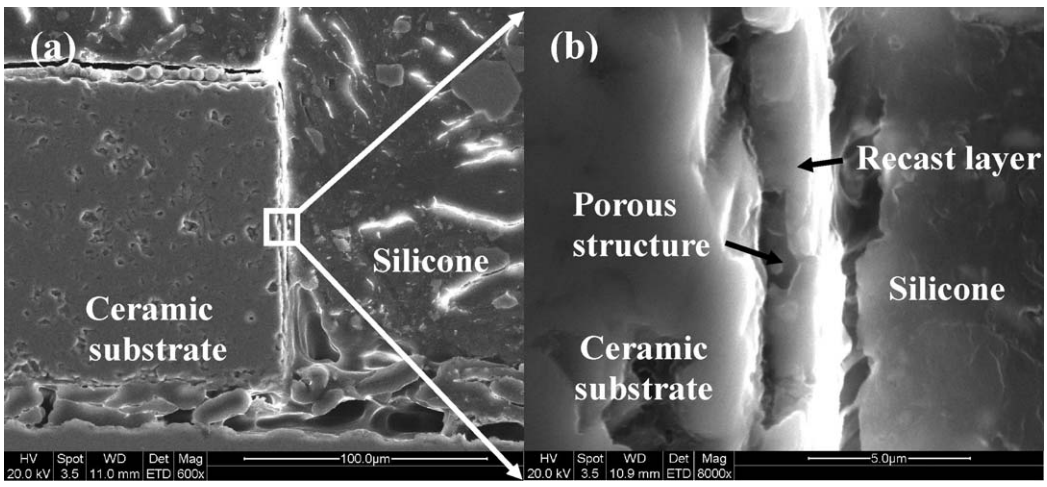

Fig. 6. Cross section of cutting groove (one side): (a) low magnification, (b) high magnification.

ous and reached a minimum at a pass delay time of 400 ms. Analysis of the orthogonal experimental results indicated that a high power density must match the high scanning speed and frequency in order to achieve both high cutting efficiency and low roughness on the sidewall. Generally, the increase in power density will result in an increase in roughness of the sidewall. However, if both scanning speed and frequency also increase as the power density increases, the roughness on the sidewall may decrease because the R_R values of both scanning speed and frequency are greater than those of the power density (Fig. 4 and Table 4). Furthermore, Fig. 4 and Table 4 also indicate that P ($R_W = 16.53$) and V ($R_W = 11.5$) were the first and second most important factors influencing the kerf width, while F ($R_W = 8.65$) and T ($R_W = 2.73$) were less important. It is concluded that a higher laser power density can increase the laser microprocessing efficiency and a higher laser scanning speed and frequency helped to significantly improve the laser microprocessing quality.

Fig. 5 shows the micrographs of the kerf top and roughness profiles on the kerf sidewall achieved by using factor combinations No. 1 and No. 4 from Table 4. When a high power density and low velocity (factor combination No. 1) was selected, the quality of laser microprocessing decreased; there was not only a wide kerf width and heat affect zone, but also micro-cracks generated in the kerf sidewall (Fig. 5(a)), and a higher roughness R_a of 1.07 μm on the kerf sidewall (Fig. 5(c)). However, when factor combination No. 4 was used, the laser microprocessing quality was improved greatly, with a narrow kerf width, no detectable micro-cracks on the surface, and a low roughness R_a of 0.24 μm (Fig. 5(b) and (d)).

Based on an overall consideration of laser microprocessing efficiency and quality, a set of optimal parameters were determined for microprocessing of ultrathin ceramics: power density of 5.09×10^6 W/cm^2, frequency of 70 kHz, laser scanning speed of 1000 mm/s, and pass delay of 400 ms.

3.2. Chemical etching results

Although the laser scanning system and multi-pass cutting mode with optimal settings were adopted to improve the UV laser microprocessing quality of ultrathin ceramic for complex graphics, it is hard to avoid or eliminate splash and debris residue on the kerf top as well as a recast layer of about 2 μm thickness on the sidewall surface (Fig. 6). In this case, the quality of laser cutting through kerf cannot reach the requirements for follow-up gilding on the kerf sidewall surface because there were many micro-cracks inside the recast layer (Fig. 7), which could cause recast layer peeling. Therefore, some other post-processing must be adopted to remove the splash and debris residue as well as the recast layer on both kerf top and sidewall surface. Two methods were considered to solve this problem; ultrasonic vibration and chemical etching. For the ultrasonic vibration, in most cases, the delicate micro-structure was very easily destroyed by the mechanical force produced by this method although recast layer could be partly removed after 1 h, as shown in Fig. 8. However, the chemical etching method could solve these issues. The processed ceramics were soaked in 100 °C concentrated sulfuric

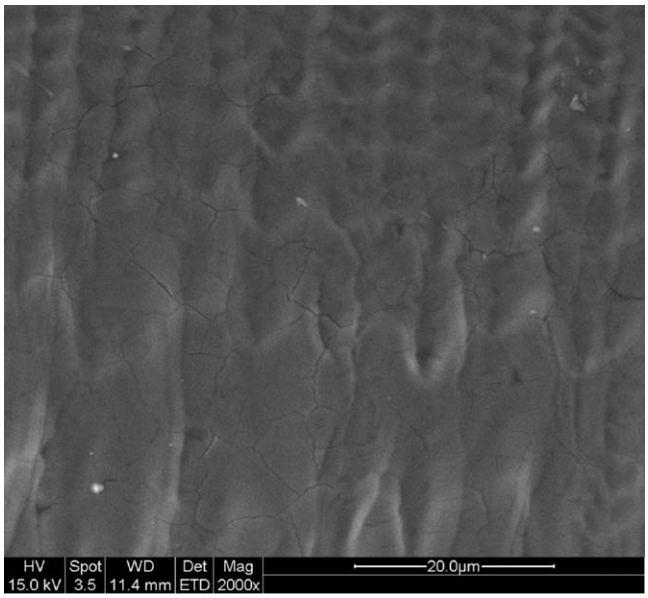

Fig. 7. Micro-cracks on the sidewall surface of the sample after laser microprocessing.

acid directly. The main chemical reaction is

$$Al_2O_3 + 3H_2SO_4 = Al_2(SO_4)_3 + 3H_2O$$

Fig. 9(a) shows the SEM micrographs of the top surface of the sample processed by the factor combination No. 1 in Table 4. There were many 1–4 μm particles remaining on the kerf edge. The more particles near the kerf edge, the larger and thicker they were. The particles could be completely removed by chemical etching, and a very clean surface could be obtained (Fig. 9(b)).

In order to investigate the influence of the concentrated sulfuric acid on the recast layer, samples were soaked in chemical solvent for different times and then examined by SEM (Fig. 10). When the samples were not chemically

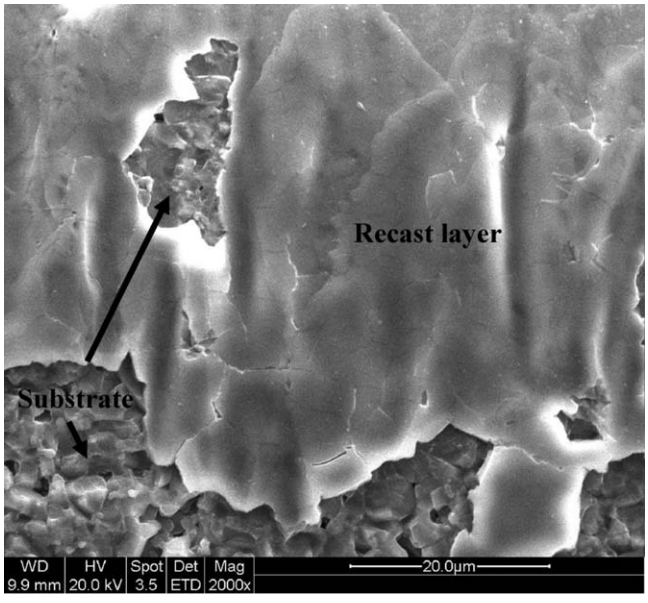

Fig. 8. Sidewall morphology of the sample after ultrasonic vibration for 1 h.

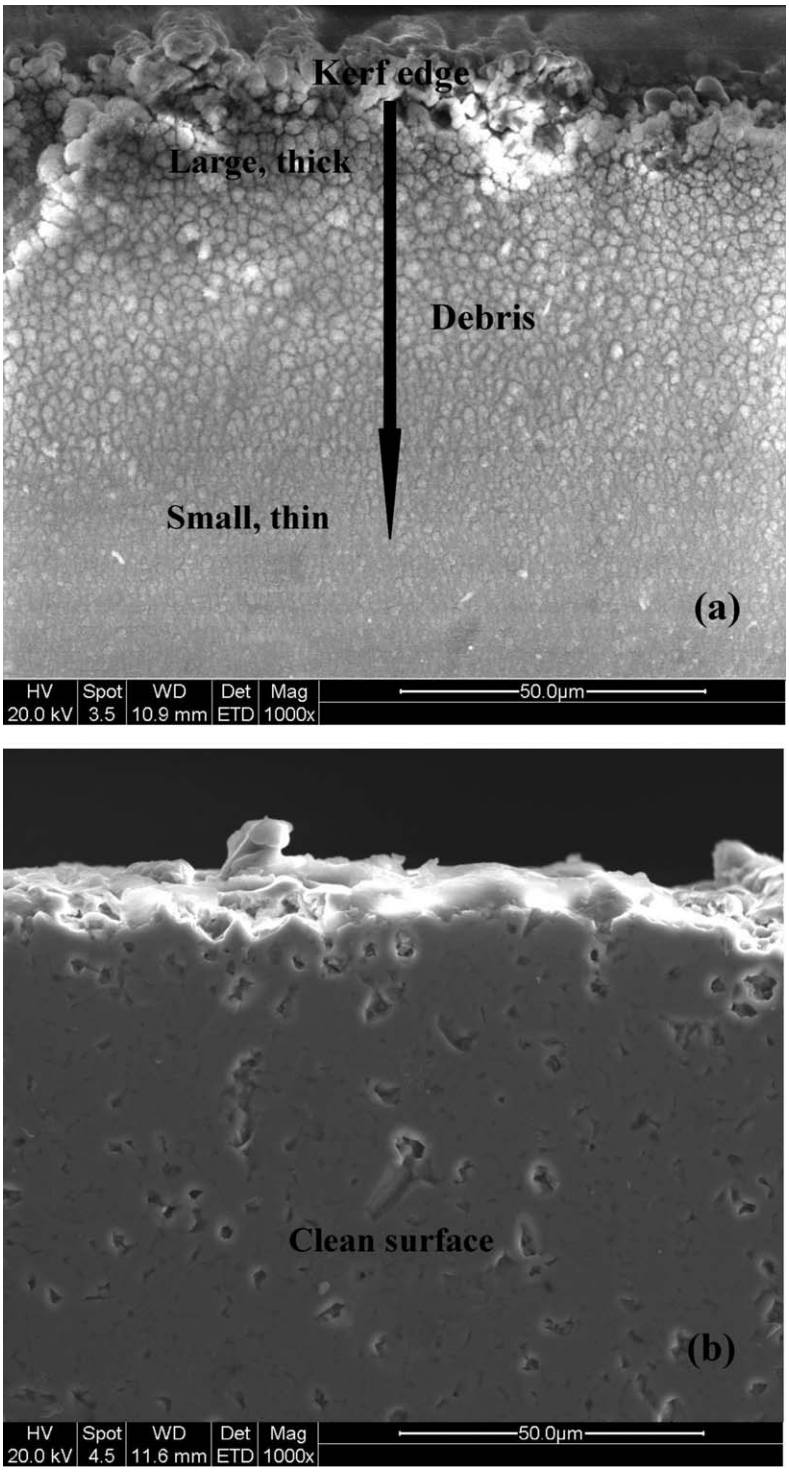

Fig. 9. Top surface morphology of the sample (a) before and (b) after soaking in concentrated sulfuric acid.

etched, there were many obvious small micro-cracks already inside the recast layer surface. The crack blocks were from a few microns to tens of microns in size (Fig. 7). After the sample was soaked in 100 °C 98% concentrated sulfuric acid for 2 h, some micro-cracks became wider and deeper (Fig. 10(a)). After 10 h, many recast layers directly fell off in blocks and the base material was exposed, as shown in Fig. 10(b) and (c). The recast layer could be removed completely after 48 h, as shown in Fig. 10(d), and the roughness R_a on the kerf sidewall dropped from 0.25 μm to 0.16 μm after the chemical treatment. Fig. 11(a) shows the final ceramic microstructure after UV laser microprocessing and chemical etching, which invested 531 s and 48 h respectively. This is a partial replicate of the microprocessing graphics shown in Fig. 3, and the high magnification of kerf edge is shown in Fig. 11(b).

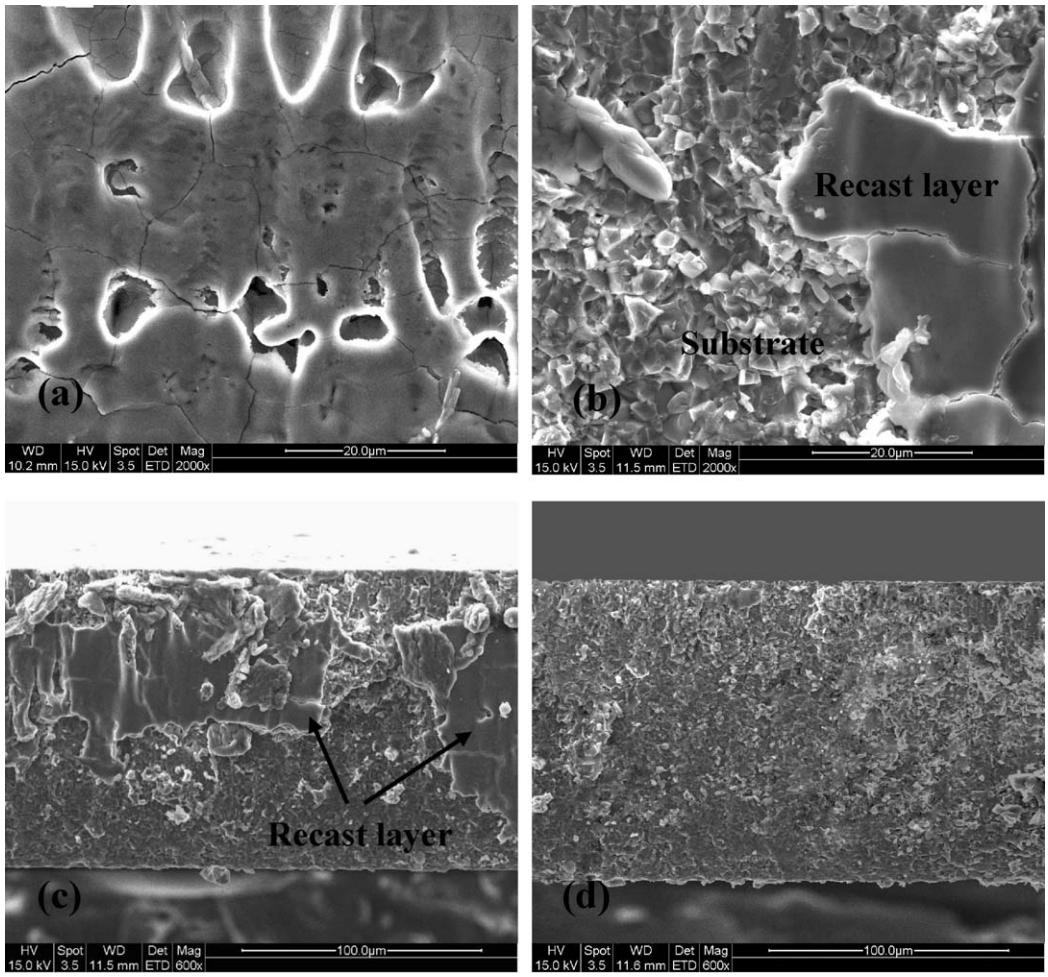

Fig. 10. SEM micrographs of a sample soaked in sulfuric acid for different times: (a) 2 h, 2000×; (b) 10 h, 2000×; (c) 10 h, 600×; (d) 48 h, 600×.

4. Discussion

The ceramic substrate material was partially melted and evaporated in the zones radiated by laser, and there was no gas jet adopted to remove the molten material as this could ruin the delicate micro-structure. Thus, there are only two mechanisms of material removal during the laser multi-scan cutting process: melt evaporation and melt ejection by the recoil pressure induced by vaporization. The ratio of evaporated to melt ejection must be large in order to achieve good laser processing accuracy and quality as this will result in less molten material ejected to form debris or a recast layer on the kerf top and sidewall. Therefore, the power density, frequency, and laser scanning speed are three key factors that influence laser microprocessing efficiency, accuracy, and quality.

Although it can increase the microprocessing efficiency greatly, the increase in power density at constant scanning speed will generate a lower ratio of evaporated to molten material and create a higher temperature gradient, resulting in more material melting during each laser scan. This will result in lower accuracy and quality, with more debris, a wider kerf width and HAZ, as well as a thicker recast layer with micro-cracks. In contrast, a higher power density matched with a higher laser scanning speed will increase the ratio of evaporated to molten material because the interaction time between laser and material is shortened. This reduces the heat diffusion time during each laser scan. In this case, the molten material produced during each laser scan will be reduced, achieving better accuracy and quality with less debris, a narrower kerf width, HAZ, and a thinner recast layer. It should be noted that the frequency will arise along with the increased laser scanning speed in order to keep the focused beam spot coupling rate at about 50%; otherwise, a coupling rate less than 50% will result in increased roughness on the kerf sidewall (and even cut though failure if the spot coupling rate is less than 0%). A suitable pass delay will benefit the processing quality. A long pass delay represents in a longer cooling time, and will result in liquid flowing downward to form a rugged surface, thus increasing sidewall roughness.There were many micro-cracks inside the recast layer caused by the thermal stress generated by the rapid cooling of molten material after laser irradiation. The micro-cracks form inside the thin recast layer and propagate perpendicularly through the recast layer to the substrate in the form of bifurcations without extending into ceramic base material. This results in a recast layer with a loose or porous structure (Fig. 6(b)) that is weakly bonded to the base, with many cracks and gaps to allow chemical solvents to enter the contact area

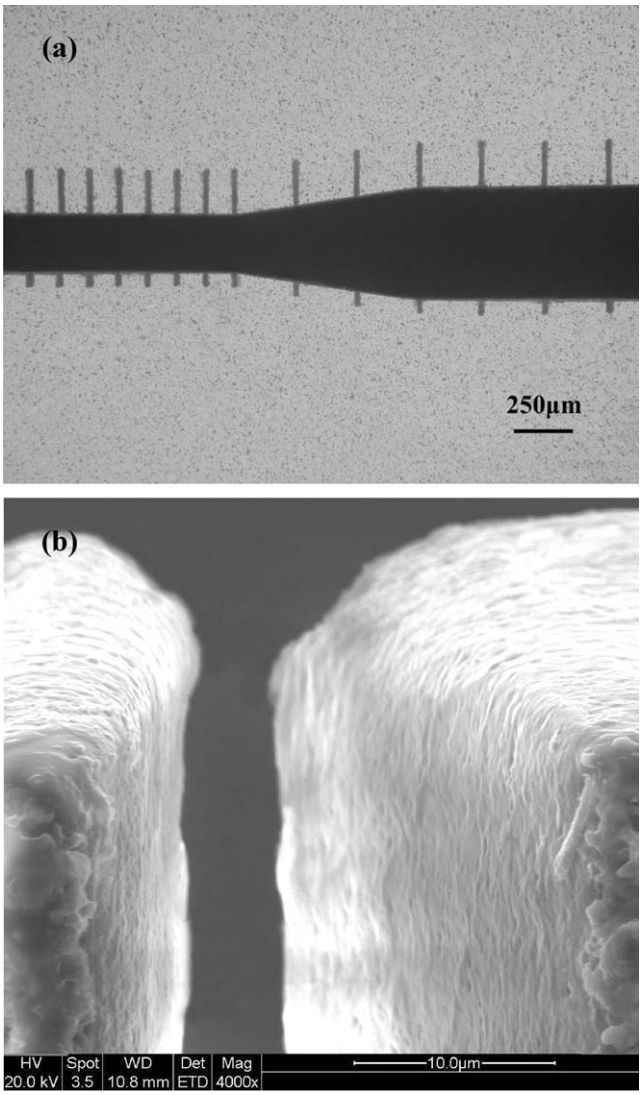

Fig. 11. (a) Partial structure of the formed sample and (b) high magnification of the kerf edge.

between the recast layer and base material. A chemical reaction based on the principle of crevice corrosion could then accelerate the process of recast layer removal. Also, the recast layer on the kerf sidewall is made up of dense and astomatous grains of α-Al_2O_3 and γ-Al_2O_3 compound,[17] and the chemically unstable γ-Al_2O_3 reacts easily with 100 °C concentrated sulfuric acid to remove the recast layer.

Therefore, a high processing quality, accuracy, and efficiency can be achieved by using UV laser cutting and subsequent chemical etching for the microprocessing of ultrathin ceramic substrate.

5. Conclusions

Delicate and complex graphics were produced on a 125 μm ultrathin ceramic substrate using UV laser microprocessing and chemical etching. A 4 × 4 orthogonal design was used to find and optimize the key laser parameters for laser microprocessing of the ultrathin Al_2O_3 ceramic substrate. After a large number of experiments using different combinations, it could be concluded that a higher laser power density combined with a suitable high scanning speed and frequency can achieve higher microprocessing efficiency, quality, and accuracy.

Chemical etching way was used to remove the splash and debris on the top surface and the thin recast layer on the kerf sidewall. This completely removed the particles after soaking and a very clean surface could be obtained. Many micro-cracks were present inside the recast layer after laser processing. After soaked in 100 °C 98% concentrated sulfuric acid for 2 h, some surface cracks became wider and deeper. After 10 h, many recast layers directly fell off in blocks from the kerf sidewall, and the recast was removed completely in 48 h. The sidewall roughness, which is dropped from 0.25 μm to 0.16 μm after the chemical treatment, finally satisfied the requirement for follow-up gilding work.

Acknowledgments

The authors gratefully acknowledge the financial supports by the National "863" Hi-Tech Research and Development Program of China (No. 2007AA030113) and the National Natural Science Foundation of China (No. 51005083).

References

1. Gillner A, Hartmann C. High-accuracy micromachining of ceramics by frequency-tripled Nd:YAG-lasers. *SPIE* 2004;**5662**:570–5.
2. Samant AN, Dahotre NB. Laser machining of structural ceramics – a review. *Journal of the European Ceramic Society* 2009;**29**:969–93.
3. Black I, Livingstone SAJ, Chua KL. A laser beam machining (LBM) database for the cutting of ceramic tile. *Journal of Materials Processing Technology* 1998;**84**:47–55.
4. Tuersley IP, Hoult TP, Pashby IR. The processing of SiC/SiC ceramic matrix composites using a pulsed Nd:YAG laser. Part I. Optimisation of pulse parameters. *Journal of Materials Science* 1998;**33**:955–61.
5. Tuersley IP, Hoult TP, Pashby IR. The processing of SiC/SiC ceramic matrix composites using a pulsed Nd:YAG laser. Part II. The effect of process variables. *Journal of Materials Science* 1998;**33**:963–7.
6. Toenshoff HK, Gonschior M. High quality laser cutting of ceramics through adapted process techniques. *SPIE* 1994;**2062**:125–35.
7. Modest MF. Minimization of elastic thermal stresses during laser machining of ceramics using a dual-beam arrangement. *Journal of Laser Applications* 2001;**13**:111–7.
8. Quintero F, Pou J, Lusquiños F, Larosi M, Soto R, Pérez-Amor M. Cutting of ceramic plates by optical fiber guided Nd:YAG laser. *Journal of Laser Applications* 2001;**13**:84–8.
9. Quintero F, Pou J, Lusquiños F, Boutinguiza M, Soto R, Pérez-Amor M. Quantitative evaluation of the quality of cuts performed on mullite–alumina by Nd:YAG laser. *Optics and Lasers in Engineering* 2004;**42**:327–40.
10. Quintero F, Pou J, Lusquiños F, Boutinguiza M, Soto R, Pérez-Amor M, et al. Comprehensive assessment of the CO_2 laser cut quality of ceramics with different assist gas injection systems. *Journal of Laser Applications* 2004;**16**:212–20.
11. Ji LF, Yan YZ, Bao Y, Jiang YJ. Crack-free cutting of thick and dense ceramics with CO_2 laser by single-pass process. *Optics and Lasers in Engineering* 2008;**46**:785–90.
12. Kurita T, Komatsuzaki K, Hattori M. Advanced material processing with nano- and femto-second pulsed laser. *International Journal of Machine Tools and Manufacture* 2008;**48**:220–7.

13. Perrie W, Rushton A, Gill M, Fox P, O'Neill W. Femtosecond laser microstructuring of alumina ceramic. *Applied Surface Science* 2005;**248**:213–7.
14. Zhu GZ, Zhu CH, Zhu X, Yuan X, Lu PX. UV laser assisted processing of ceramics in air and in water. *SPIE* 2005;**5629**:309–13.
15. Tsai CH, Li CC. Investigation of underwater laser drilling for brittle substrates. *Journal of Materials Processing Technology* 2009;**209**:2838–46.
16. Li L, Achara C. Chemical assisted laser machining for the minimisation of recast and heat affected zone. *CIRP Annals – Manufacturing Technology* 2004;**53**(1):175–8.
17. Wang XY, Xu WJ, Lei MK, Chen H, Wang LJ, Guo DM. An experimental study of laser milling based on deteriorative layer on Al_2O_3 ceramic. *Journal of Dalian University of Technology* 2009;**49**(2):211–5.